chapter in
Mechanics and Physics of Solids at Micro- and Nano-Scales

Edited by
Ioan R. Ionescu, Sylvain Queyreau, Catalin R. Picu, Oguz Umut Salman

WILEY

7

Surface Effects on Elastic Structures

7.1. Introduction

Classical continuum elasticity is scale invariant: as long as proportions are kept constant, the size of an object does not matter in regard to elastic deformations. For example, buckling of a structure of a given shape would occur for the same imposed strains, independently of its size. We would, therefore, expect the same phenomena observable at the macroscopic scale to occur at the micro-scale (and maybe even at the nano-scale so long as continuum approximation holds).

However, the presence of a surface energy γ modifies this picture by introducing a length scale to the problem. In particular, the coupling between surface interactions and elasticity is characterized by a length scale that compares the force per unit length exerted by the surface effect to the rigidity of the solid: $\ell_{ec} = \gamma/E$, where E is Young's modulus of the material. In this situation, the size L of the system, therefore, matters, and a structure bigger than ℓ_{ec} is insensitive to surface effect, while a smaller structure might be strongly deformed. In fact, we show that for slender structures, even when $L \gg \ell_{ec}$, large deflections may still occur because slenderness implies a weak stiffness in bending.

In this chapter, we are interested in how two different surface effects can deform elastic structures. We start with the interaction between capillary surface tension and slender mechanics, and how a droplet can deform a thin

Chapter written by Hadrien BENSE, Benoit ROMAN and José BICO.

sheet. We then focus on electrostatic surface effects and their use to actuate electroactive polymer membranes.

7.2. Liquid surface energy

In this first part, we show how the surface tension of a liquid interface in contact with an elastic solid may deform it. Recent years have seen a large body of research effort in this field. Here we only give scaling arguments and present the consequences of a surface tension force at the micro-scale. Thorough reviews are available (see, e.g. Andreotti and Snoeijer in press; Bico *et al.* 2018).

7.2.1. *Can a liquid deform a solid?*

Surface tension is the surface energy cost, γ, associated with the creation of an interface between two materials (be they liquid or solid). γ is positive: surface tension tends to minimize the area of an interface. These capillary interactions are responsible for a large number of phenomena in liquids, such as imbibition, the motion of insects at the surface of water, and the spherical shape of small drops and bubbles (de Gennes *et al*. 2002).

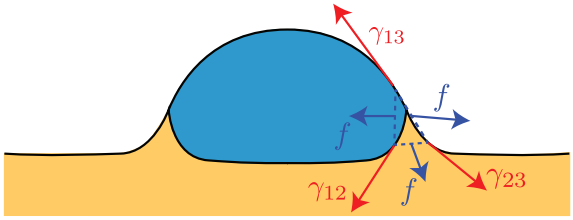

Figure 7.1. *Deformation of a solid by a liquid. For a color version of this figure, see www.iste.co.uk/ionescu/mechatronics.zip*

In this section, we are interested in how surface tension can deform a solid that is not slender. Consider, for example, the effect of a droplet deposited on a solid: it exerts a torque on the latter. Indeed, the air/liquid surface tension pulls up the solid (γ_{13} in Figure 7.1), while the Laplace pressure pushes down (note that Laplace pressure ensures the vertical equilibrium of forces in the drop,

and the horizontal projection leads to the classical Young–Dupré's relation) so that the solid may deform (Lester 1961). However, taking a standard value of $\gamma \approx 70\ mN/m$ for liquid water, and Young's modulus on the order of 70 GPa for the solid (typically glass), one finds that the fluid can deform the solid on a length scale on the order of $\gamma/E \approx 1$ pm. At such a small scale (smaller than intermolecular distances), the use of continuum mechanics is dubious, and such elasto-capillary effects are irrelevant. However, the recent development of microfabrication methods, ultra soft gels, and observation techniques have led to the study of the coupling between capillary forces and elasticity. For example, the deformation near the contact line of a droplet lying on a very deformable substrate ($E \approx 3$ kPa) has been observed with confocal microscopy. It has been shown that the substrate adopts a shape that does not depend on its thickness nor on the droplet size, but only on the liquid composition (Style *et al*. 2013). Another example is the rounding off of extremely soft gels (shear modulus between 35 and 350 Pa). These gels are casted with sharp angles, but the surface tension of the solid softens the corners so that they exhibit a curvature on the order of E/γ (see Mora *et al*. 2013). This experimental observation of the action of a solid's surface tension has led to many numerical and theoretical developments.

In conclusion, we have seen that a liquid can deform a solid in its bulk, but only at a very small scale, and for very soft solids. However, we will show that on *slender* structures, surface or capillary effects may produce macroscopic deformations, even in materials with a high Young's modulus.

7.2.2. *Slender structures*

A slender structure is a structure with at least one dimension that is small when compared to the others. A plate, for example, has a very small thickness h compared to its length L and width w. Due to their slenderness, these structures can be considered with two modes of deformation. On the one hand, the structures can undergo stretching (or equivalently compression), with an elastic energy

$$\mathcal{E}_{stretch} \simeq EhLw\epsilon^2$$

for an in-plane strain ϵ, where E is Young's modulus of the plate (left scheme in Figure 7.2).

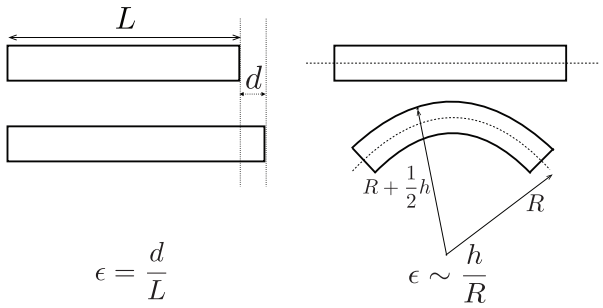

Figure 7.2. *The two modes of deformation of a slender structure: stretching (left) and bending (right)*

On the other hand, the plate can be given a radius of curvature R. The bending energy associated with this deformation is

$$\mathcal{E}_{bend} \simeq \frac{B}{R^2} LW,$$

where $B \simeq Eh^3$ is the bending stiffness of the plate (right scheme of Figure 7.2). Stretching energy is, therefore, proportional to the thickness h, whereas bending energy is proportional to h^3. Consequently, the bending energy of a thin structure (small thickness h) vanishes very quickly when the thickness vanishes. What are the practical consequences of this very compliant mode of deformation?

7.2.3. *Wrapping a cylinder*

A simple way to understand how surface forces may bend a slender structure is to consider a solid cylinder of radius R, covered with a liquid of surface tension γ, and a sheet of thickness h. We assume the liquid to perfectly wet both solids. What are the conditions for the sheet to spontaneously wrap the cylinder (Figure 7.3)? Wrapping occurs if surface tension is strong enough to bend the sheet with a radius of curvature R. This is a pure bending problem, and the energetic cost associated with this deformation is proportional to $Eh^3 \frac{Lw}{R^2}$. However, covering the cylinder with the sheet reduces the interface between the liquid and the air, and thus is energetically favorable. The associated energetic gain is $2\gamma Lw$. These two energies are in competition, and wrapping will be possible when the energetic gain due the reduction of the

air/liquid interface is higher than the energetic cost of the elastic deformation of the sheet, i.e. when

$$E\frac{h^3 Lw}{R^2} < 2\gamma Lw.$$

This condition can be expressed in terms of a cylinder critical size:

$$R > \ell_B = \sqrt{\frac{Eh^3}{\gamma}},$$

where ℓ_B is the capillary-bending length, the relevant length scale when dealing with bending deformations of slender structures by capillary effects. It compares the bending stiffness of the elastic structure to the surface tension of the liquid. If a cylinder has a radius smaller than this length, surface tension will not be able to sufficiently deform the sheet for wrapping to occur.

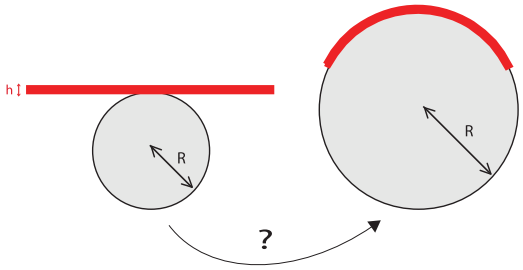

Figure 7.3. *Can a thin sheet wrap around a wet cylinder?*

Elasto-capillary deformation is not simply an interesting academic problem, it also has practical consequences in the field of microfabrication. Indeed, the main technique used to manufacture microelectromechanical systems (MEMS), or micro-electronic elements, is photolithography. After an insulation step, a photo-sensitive resin is put into a solvent solution. During the drying process, capillary bridges may form inside these objects, which can cause deformations, stictions, or even fractures. These irreversible events are strong limiting factors in the elaboration of slender microstructures, such as nanolines, microcantilevers, or microstamps (Hui *et al*. 2002; Namatsu *et al*. 1995; Tas *et al*. 1997).

7.2.4. *Capillary origamis*

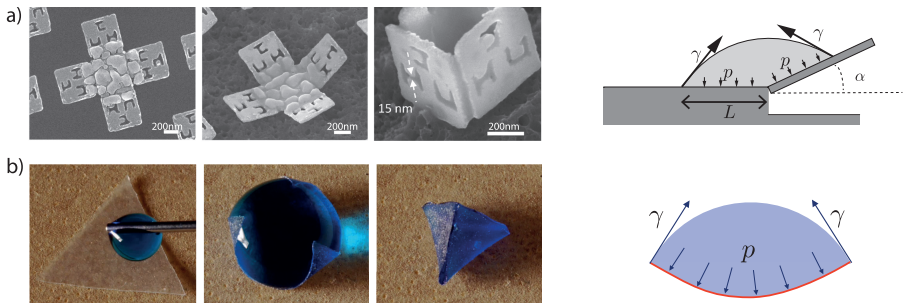

Figure 7.4. *a) Cubic boxes obtained after the fusion of the welding deposited on the hinge of the initial pattern (taken from Cho* et al. *2010); b) Capillary origami Py* et al. *(2007)*

Manufacturing 3D structures at a micro-scale with classical microfabrication techniques is a very complicated task, partly because of the limiting role played by surface tension. This force can also be harnessed. The top row of Figure 7.4(a) presents the examples of micrometer cubes obtained, thanks to capillary interactions. A liquid metal droplet is deposited at the hinge of an initially flat metallic sheet, and as it tends to minimize its interface with the air, it folds the cube (see scheme 7.4(a) and Cho *et al*. 2010). We will focus on the technologically simpler case where a macroscopic sheet is deformed by a droplet (Figure 7.4(b)). What happens when a water droplet is deposited on a thin polymer sheet? Does the drop spread, or does the sheet wrap the droplet? If, for example, the droplet is deposited on a 50-μm-thin silicone elastomer square sheet, we first observe that the corners of the sheet wrap the droplet. As the liquid evaporates, the sheet bends more and more until its complete closing (see Figure 7.4). Once the droplet has completely evaporated, the sheet may return to its flat state, or remain curved, depending on the intensity of Van der Waals interactions. How do the capillary forces act on the sheet? On the one hand, liquid/air surface tension exerts a traction that pulls the sheet up; on the other hand, Laplace pressure exerts a pressure that pushes the sheet down (the drop being curved, the pressure inside the liquid is higher than outside). The drop is, therefore, exerting a moment on the sheet (scheme in Figure 7.4(b)). The capillary torque scales as γL^2, while the typical torque

to bend the sheet on its own size scales as $B \simeq Eh^3$. Therefore, we expect wrapping if the sheet exceeds the size limit:

$$L_{crit} \simeq \sqrt{\frac{B}{\gamma}} \simeq \ell_B.$$

Experiments have been carried out with sheets of different thicknesses and different shapes (triangles or squares). In each case, the critical length has been determined. L_{crit} is indeed found to be proportionnal to ℓ_B, with a prefactor that depends on the geometry of the sheet: $L_{crit} \approx 12\ell_B$ for triangles and $L_{crit} \approx 7\ell_B$ for squares (see Py *et al*. 2007).

Interestingly, this law holds up to nanometric scales as shown with simulations on graphene sheets (see Patra *et al*. 2009). At a higher scale, gravity starts to play a role, and the maximal size is fixed by the capillary length. Finally, the initial shape of the sheet can be tuned to obtain different 3D shapes, as illustrated in Figure 7.5.

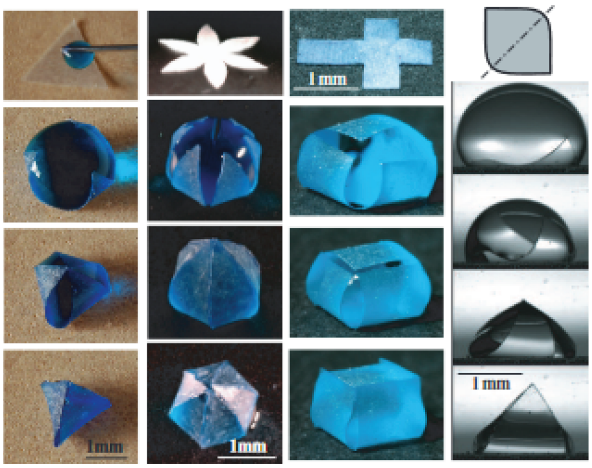

Figure 7.5. *Different patterns lead to different 3D shapes. For a color version of this figure, see www.iste.co.uk/ionescu/mechatronics.zip*

In this first part, we studied how a liquid can deform a solid through surface tension interactions. We focused on the interplay between the peculiar mechanics of slender structure and surface tension. The slenderness of

the structure is what allows the surface tension to produce remarkable deformation, even though γ/E remains very small. As we explained earlier, the addition of surface effects brings new length scales to problems that would otherwise be scale invariant. More precisely, we have seen that the relevant length scale when dealing with slender structure interacting with capillary forces is the capillary bending length ℓ_B. This length captures the slender elasticity by comparing the bending rigidity to the surface tension. In the following, we examine the deformation of thin plates mediated via an electrostatic surface energy.

7.3. Dielectric elastomers: a surface effect?

We now focus on the description of dielectric elastomers, with an emphasis on electrostatic interactions seen as a surface effect, which play an important role.

7.3.1. *Introduction: electrostatic energy of a capacitor as a surface energy*

These last years have seen the rapid development of a novel class of robotics made of a compliant material called "soft robotics". Electroactive polymers are, among the possible technologies to build such robots, a particularly cost-effective and easy-to-manufacture technology. The large deformation electroactive materials can achieve up to 500% in area strain (Huang *et al*. 2012), and their harmless contact make them suitable for a wide range of potential applications: from bioinspired actuators (Carpi *et al*. 2005; Carpi and Rossi 2007) to soft grippers (Araromi *et al*. 2015; Shintake *et al*. 2016), or tunable lenses (Carpi *et al*. 2011; Maffli *et al*. 2015; Son *et al*. 2012), and even energy harvesting systems (Foo *et al*. 2012; Kaltseis *et al*. 2011; McKay *et al*. 2011). Although their rediscovery is certainly recent, the principle of dielectric actuation can be traced back to Röntgen (Keplinger *et al*. 2010) at the end of the 19th Century. The basic idea is indeed fairly simple: a dielectric elastomer is a soft capacitor, in which both electrodes and the insulating material can deform under the action of Coulombian interactions (see Figure 7.6(a)). Charges from the opposite faces of the membrane attract each other, leading to a reduction of its thickness and, therefore, to in-plane extension. However, a surface effect is also at play in this system. Indeed, the electrostatic energy

$\mathcal{E}_{els}$ of a planar capacitor whose electrodes are separated by H and have a surface S reads:

$$\mathcal{E}_{els} = -\frac{1}{2}\varepsilon\frac{V^2}{H}S \qquad [7.1]$$

where ε is the permittivity and V is the potential difference. For a fixed gap H, this energy is proportional to the area of the electrode and can, therefore, be seen as a (negative) surface energy, which would tend to increase the surface S.

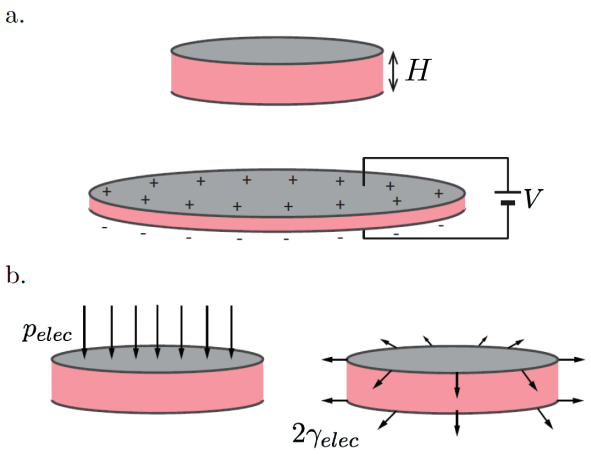

Figure 7.6. *a) An electroactive polymer setup is made of two compliant electrodes separated by a dielectric polymer. When a voltage is applied, the area of the electrodes increases. b) The electrostatic interactions can be decomposed in two effects: an electrostatic pressure, acting through the thickness of the membrane, and a negative surface tension, acting along the membrane*

To gain intuition on this surface term, we can evoke electrowetting. Lipmann, during his PhD (Lippmann 1875), imposed a potential difference V between a conductive drop and a metallic surface separated by a dielectric layer (see Figure 7.7) with thickness H. The drop is observed to spread, and we can interpret this as a result of the repulsion of charges with the same sign at its surface. It is as if the electric field was modifying the drop surface tension γ into: $\gamma' = \gamma - \frac{1}{2}\varepsilon\frac{V^2}{H}$. More precisely, the electric field reduces the apparent surface tension compared with the initial one, and therefore, it seems that its effect can be represented as forces localized at the liquid interface.

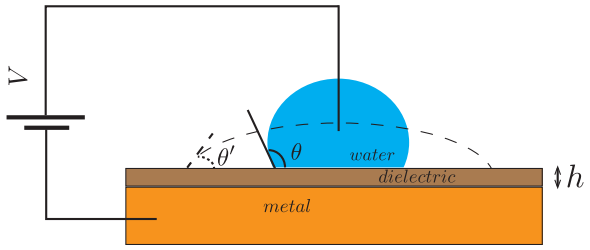

Figure 7.7. *Electrowetting: under the application of a voltage, the drop spreads*

In the case of an electroactive polymer (Figure 7.6), the material expanding is a solid unlike in the electrowetting experiment, but similar line forces are expected to take place at the boundary of the electrode. We wish to clarify the consequences of such a negative surface tension (with an electrostatic origin) in this elastic solid.

In this chapter, we intend to sketch the formal derivation of the equilibrium equations of an electroactive polymer, with an emphasis on the case where the electrodes are not entirely covering the membrane. In doing so, we will shed light on the practical consequences of the tensile stress existing in the system, and its physical origin, by drawing analogies with capillary surface tension. The rationale developed in this first part will then be applied to an experimental study of a buckling instability triggered by inhomogeneous actuation of the system.

7.3.2. *Mechanics of dielectric elastomers*

Our approach derives the equations for the deformation of the polymer under an electric field through a variational approach. We compute both the elastic and electrostatic energies and minimize the total energy to obtain the equations coupling electrostatics and elasticity. We will then give several interpretations of these equations.

For simplicity, we will consider the planar case of a dielectric strip of thickness H, width W, and length L at rest. In this reference state, the system is parametrized with the curvilinear abscissa S and the coordinates X, Y, and Z running, respectively, along the length, width, and thickness of the strip. Upper case letters refer to the reference, undeformed state, and lower case

letters refer to the deformed state. We assume small strains $e \ll 1$ and a plane strain configuration: $e_y = 0$ (a plane stress configuration with $\sigma_{yy} = 0$ would not qualitatively change the results). A more detailed derivation and discussion is the subject of a future article by Bense *et al*.

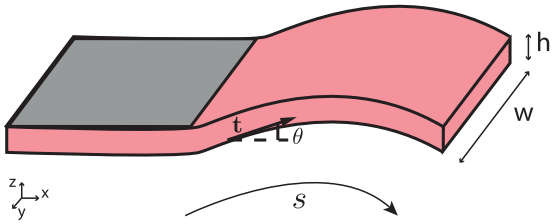

Figure 7.8. *Scheme of a partially activated dielectric elastomer. The grey part represents the electrode. For a color version of this figure, see www.iste.co.uk/ionescu/mechatronics.zip*

In the deformed state, the curvilinear coordinate is denoted as s and θ is the local slope (see Figure 7.8). We introduce the tangential strain averaged over the thickness of the membrane e_t, which determines the stretching:

$$ds = (1 + e_t)dS$$

Similarly, we define the average normal strain e_n as:

$$h = (1 + e_n)H$$

And finally, the curvature:

$$\kappa = \frac{d\theta}{ds} = \frac{1}{1 + e_t}\frac{d\theta}{dS} \approx \frac{d\theta}{dS}$$

With the small strains and slender-body approximations, the latter indeed means that the curvature is small: $(H\kappa)^2 \ll 1$. We can, therefore, neglect any nonlinear term involving products of both κ and e_t or e_n.

7.3.2.1. *Elastic energy*

In the case of plane strain assumed here (where there is no strain along direction Y), Hooke's law leads to the in-plane stretching energy per unit surface of the strip, depends on the tangential and normal strains (e_t, e_n) and reads

$$\mathcal{E}_{stretch} = \frac{1}{2}\mathcal{Y}\left(e_t^2 + \frac{2\nu}{1-\nu}e_n e_t + e_n^2\right),$$

where we have introduced the effective stretching modulus

$$\mathcal{Y} = \frac{(1-\nu)EH}{(1-2\nu)(1+\nu)} \qquad [7.2]$$

This expression takes an unusual form because the variation of thickness e_n appears here as an unknown. It is indeed customary in thin-plate mechanics to assume that stresses on the faces of the plate vanish, thus setting the value of $e_n = -\nu/(1-\nu)e_t$ (for this case of plane strain) and $\mathcal{E}_{stretch} = \frac{1}{2}\frac{EH}{1-\nu^2}(e_n)^2$. Following this, the in-plane force per unit distance (or tension) $T = \frac{EH}{1-\nu^2}e_t$ would be proportional to stretching strain, as expected. We find that electrostatic pressure on the faces is not negligible, and they play an important role, modifying the relation between tension T and deformation e_t.

The bending energy per unit surface takes, however, the usual form

$$\mathcal{E}_{bend} = \frac{1}{2}B\theta'^2, \text{where the bending stiffness is } B = \frac{EH^3}{12(1-\nu^2)}. \qquad [7.3]$$

7.3.2.2. *Electrostatic energy*

The electrostatic energy of the system comprising the electroactive polymer and the generator imposing a fixed voltage V writes $\mathcal{E}_{els} = -\frac{1}{2}CV^2$. In order to take the curvature of the capacitor into account, we consider the capacity of a capacitor formed by two coaxial cylinders:

$$C = \frac{2\pi\varepsilon w}{\ln\left(\frac{1+\kappa h/2}{1-\kappa h/2}\right)}, \qquad [7.4]$$

where ε is the dielectric constant of the polymer. We expand [7.4] for small curvatures $\kappa h \ll 1$ to find the expression for the electrostatic energy (per unit width) in the slender-body approximation:

$$\mathcal{E}_{els} = -\int ds\, \frac{\varepsilon}{2}\frac{V^2}{h}\left[1 - \frac{1}{12}(h\kappa)^2\right]. \qquad [7.5]$$

This energy is a generalization of equation [7.1] and is still proportional to the surface (remember $\mathcal{E}_{els}$ above is written per unit width), making it

analogous to a surface tension with a negative sign. Moreover, we notice a term proportional to the curvature κ^2, analogous to a elastic bending rigidity in equation [7.3]. The associated electrostatic bending modulus is:

$$B_V = \frac{\varepsilon V^2 h}{12} \simeq \frac{\varepsilon V^2 H}{12}, \qquad [7.6]$$

at leading order in strain. Finally, to simplify the following calculations, we express the electrostatic energy in the reference coordinate and as a function of $e_n(S)$, $e_t(S)$, and $\theta(S)$:

$$\mathcal{E}_{els} = -\frac{\varepsilon}{2}\frac{V^2}{H}\int dS\,\frac{1+e_t}{1+e_n} + \int dS\,\frac{1}{2}B_V\theta'^2. \qquad [7.7]$$

7.3.2.3. *Variations*

We assume here, for the sake of simplicity, that both end positions of the strip are fixed. The details of the boundary conditions may not affect the main results of our discussion. The end point position measured from the origin, therefore, reads:

$$\mathbf{r}_{\text{end}} = \int dS\,(1+e_t)\mathbf{t}, \qquad [7.8]$$

where $\mathbf{t}$ is a unit vector tangent to the sheet (having, therefore, an angle θ with the x axis). This constraint will be imposed with a Lagrange multiplier $\mathbf{f}$, which corresponds to an externally applied force. Finally, the total energy to be minimized is

$$F = \int dS\,\mathcal{F}(e_t, e_n, \theta), \qquad [7.9]$$

with the surface density of energy given by the sum of all contributions

$$\mathcal{F}(e_t, e_n, \theta) = \frac{1}{2}\mathcal{Y}\left(e_t^2 + \frac{2\nu}{1-\nu}e_n e_t + e_n^2\right) + \frac{1}{2}(B+B_V)\theta'^2 - \frac{\varepsilon}{2}\frac{V^2}{H}\frac{1+e_t}{1+e_n} - (1+e_t)\mathbf{f}\cdot\mathbf{t}, \qquad [7.10]$$

where this expression must be used with $B_V = 0$ and $V = 0$ in the portion of the strip that is not covered by the electrode. We now minimize this functional with respect to different parameters to obtain the set of equilibrium equations:

$$\frac{\delta F}{\delta \theta(S)} = -(B + B_V)\theta'' - (1 + e_t)\mathbf{f} \cdot \mathbf{n} = 0, \quad [7.11]$$

$$\frac{\delta F}{\delta e_n(S)} = \mathcal{Y}\left(e_n + \frac{\nu}{1-\nu}e_t\right) + \frac{\varepsilon}{2}\frac{V^2}{H}\frac{1+e_t}{(1+e_n)^2} = 0, \quad [7.12]$$

$$\frac{\delta F}{\delta e_t(S)} = \mathcal{Y}\left(e_t + \frac{\nu}{1-\nu}e_n\right) - \frac{\varepsilon}{2}\frac{V^2}{H} - \mathbf{f} \cdot \mathbf{t} = 0. \quad [7.13]$$

These equations are geometrically nonlinear and, as such, are valid for large displacements. In the remainder of this section, we will consider small strains and, therefore, replace $1 + e_n \approx 1$ and $1 + e_t \approx 1$.

Equations [7.11] and [7.13] can be interpreted as force balance equations projected, respectively, along the normal and tangential directions. Defining $T = \mathbf{f} \cdot \mathbf{t}$ as the membrane tension (which may be compressive if negative) and $\mathcal{P}$ as the electrostatic pressure, as the usual attractive pressure between two parallel conducting plates.

$$\mathcal{P} = \frac{\epsilon}{2}\frac{V^2}{H^2}, \quad [7.14]$$

Combining equations [7.11] and [7.13] to eliminate e_t, we can obtain the following equation governing the tangential strain e_t:

$$T = \frac{EH}{1-\nu^2}e_t - \frac{1}{1-\nu}H\mathcal{P}. \quad [7.15]$$

The total tension may be decomposed into the usual elastic tension of the membrane (first term, following the usual Hooke's law) and a compressive (negative) tension induced by electrostatics (second term). Similarly, we can compute the normal strain e_n, which reads:

$$\frac{EH}{1-\nu^2}e_n + \frac{1}{1-\nu}H\mathcal{P} = -\frac{\nu}{1-\nu}T. \quad [7.16]$$

Note that equations [7.15] and [7.16] are equally valid in the regions without electrode by taking $\mathcal{P} = 0$.

These two equations unveil the first effect of the electro-actuation: at the boundary between the covered and non-covered membranes as the electrostatic pressure $\mathcal{P}$ drops to zero, the strains e_t and e_n are discontinuous. This discontinuity is also naturally observed in the stresses, if computed from these strains using Hooke's law, which we will discuss in section 7.3.2.4.

In equation [7.11], we also recognize the standard Elastica equation (Love 2011) for a strip submitted to a force $\mathbf{f}$ at its end:

$$(B + B_V)\theta'' + \mathbf{f} \cdot \mathbf{n} = 0, \qquad [7.17]$$

with a difference in the added electrostatic bending rigidity B_V (valid only in the electroactive region).

The energy minimization that we performed, therefore, shows us that the peculiar mode of actuation of this plate does not modify the global buckling equation (apart from an added bending rigidity). Nonetheless, it introduces a discontinuity in the stress and strain fields at the boundary between the electrode and the membrane (although the total force transmitted through the membrane $\mathbf{f}$ is continuous). In the following, we propose several interpretations of these equations.

7.3.2.4. *Electrostatic surface tension and pressure*

Qualitatively, the electrostatic interactions can be thought of as giving rise to two effects. On the one hand, the attraction of opposite sign charges between the faces of the dielectric generates an electrostatic pressure that compresses the membrane along its thickness. This effect can be made apparent by manipulating the force balance along the $\mathbf{z}$ axis (equation [7.16]). Indeed, let us assume, for example, that no external force is applied to the membrane, i.e. $T = 0$, and then, using Hooke's relation, equation [7.16] can be rewritten as:

$$\sigma_{zz} = -\mathcal{P} = -\frac{1}{2}\frac{\varepsilon V^2}{h^2}.$$

This compressive stress of electrostatic origin is the classical Maxwell pressure that acts on a rigid plate capacitor. Through the Poisson effect, this pressure contributes to the extension of the membrane.

On the other hand, repulsion of the same sign charges on each electrode creates a tensile stress. Similarly, equation [7.15], equilibrium of longitudinal

forces, can be rewritten in the absence of externally applied membrane tension $T = 0$,

$$\sigma_{xx} = \mathcal{P} = \frac{1}{2}\frac{\varepsilon V^2}{h^2}.$$

An electrostatic positive (tensile) stress, of equal magnitude as the electrostatic pressure, acts along the electrode and helps its expansion. As a result, the system undergoes a compressive stress across its thickness and a tensile stress along its electrode (see Figure 7.6), leading to the strain derived in equations [7.15] and [7.16]. Interestingly, both effects have the same magnitude.

We may now comment on the discontinuities in the elastic stresses at the electrode boundary for a strip submitted to a total membrane force T. The discontinuity in σ_{zz} simply results from the fact that an electrostatic pressure $\sigma_{zz} = \mathcal{P}$ is applied under the electrode, whereas $\sigma_{zz} = 0$ outside, where the electrostatic pressure vanishes. The situation is more subtle for the in-plane stresses σ_{xx}. Applying [7.15] inside and outside the electrode and using Hooke's law, we can deduce the value of the elastic stresses jump $\Delta\sigma_{xx} = \mathcal{P} = \frac{\epsilon}{2}\frac{V^2}{H^2}$. This jump results from a localized force at the boundary of the electrode $\frac{\epsilon}{2}\frac{V^2}{H}$, consistently with the negative surface tension deduced from [7.1].

We conclude that elastic stress in the material results from (i) an electrostatic pressure on its faces and (ii) a surface tension force acting on the boundaries of the electrode. We propose different interpretations of these stress distributions in the next two sections.

7.3.2.5. *Doubled electrostatic pressure*

A very common approach to describe electroactive polymers was introduced by Ronald Pelrine in his seminal work (Pelrine *et al.* 1998). To better understand, let us consider a strip subjected to a simple **mechanical pressure** $\sigma_{zz} = -\mathcal{P}_0$ on one specific region. In that case, Hooke's relations lead to:

$$T = Hw\left(\frac{1}{1-\nu^2}Ee_t - \frac{\nu}{1-\nu}\mathcal{P}\right) \qquad [7.18]$$

If we now compare equation [7.15] (electrostatic actuation) and equation [7.18] (mechanical actuation), we note that both equations are equivalent (i.e.

electrostatic and mechanical actuations produce the same strain) if $\mathcal{P}_0 = \mathcal{P}/\nu$. In the common case where the dielectric polymer is an elastomer, we have $\nu = 0.5$. For an electroactive elastomer, the state of strain under actuation can, therefore, be derived by considering that a doubled electrostatic pressure acts on the system, without any negative surface tension effect. Our variational approach agrees that this point of view is still valid in the case where the electrodes do not entirely cover the membrane. This approach is simpler when one is interested in the strain field in the membrane. However, the state of stress and the added electrostatic bending rigidity are missed.

7.3.2.6. *Equivalent growth*

Equations [7.15] and [7.16] can be rewritten as:

$$T = \frac{EH}{1-\nu^2}(e_t - e_t^0) \qquad [7.19]$$

$$\frac{EH}{1-\nu^2}(e_n - e_n^0) = -\frac{\nu}{1-\nu}T, \qquad [7.20]$$

if we define

$$e_t^0 = (1+\nu)\frac{\mathcal{P}}{E}; \qquad e_n^0 = -(1+\nu)\frac{\mathcal{P}}{E}. \qquad [7.21]$$

Written in this way, these equations are exactly the ones describing an elastic strip whose reference state differs by a strain (e_t^0, e_n^0) from the initial stress-free reference sate. By reference state, we mean that the state was obtained without external mechanical loading $T = 0$. This rewriting, therefore, provides another interpretation of the electrostatic loading: applying a voltage is equivalent to defining a new stress-free reference state for the membrane. This situation is similar to the cases of inelastic strain, such as those produced by growth or plastic deformation, which effectively redefines the reference state. Hence, the electrostatic loading can be seen as a modification of the rest length of the strip, together with providing a new bending rigidity $B + B_V$. This interpretation differs from other common approaches such as those described earlier. It presents the advantage of completely capturing the electrostatic effects and provides a useful framework when dealing with non-homogeneous actuation.

7.3.2.7. *Conclusion and order of magnitude*

In this section, we demonstrated how the electrostatic loading can be decomposed in two effects, first, a compressive pressure

$$\mathcal{P} = \frac{1}{2}\frac{\varepsilon V^2}{H^2}$$

on the faces of the electrode, and second, a (negative) surface tension

$$\gamma = -\frac{1}{2}\frac{\varepsilon V^2}{H}. \qquad [7.22]$$

on the electrode. Both effects tend to expand the membrane, with the same order of magnitude (in fact, for $\nu = 1/2$, both effects produce the exact same strain).

Referring to the introduction of this chapter, we may estimate the effect of, say, the surface tension term by computing the electrostatic equivalent to the bulk elasto-capillary length γ/E, in which γ designates the electrostatic surface tension defined in [7.22], $\gamma = \frac{\varepsilon}{E}\frac{V^2}{H}$. In typical experiments, we find $\gamma/E = H\mathcal{P}/E \approx 10^{-6}$ m. As for the capillary case, this length scale is too small to play an important role in the problem. In fact, $\mathcal{P}/E$ can be interpreted as the typical strains in the material, which remain modest and do not induce large shape change.

However, we get into the detailed study of a specific example that mechanical instabilities can be harnessed in an electro-actuated thin membrane to obtain interesting shape changes.

7.3.3. *Buckling experiments*

We experimentally investigate how a non-uniform spatial distribution of voltage can trigger out-of-plane buckling patterns in electro-activated polymers. This work is inspired by non-uniform growth of plant leaves or material swelling that leads to complex 3D shapes (Dervaux and Ben Amar 2008; Klein *et al*. 2007; Kim *et al*. 2012; Wu *et al*. 2013).

We focus on a model axisymmetric configuration where a circular membrane floats freely on a bath of water. A compliant circular electrode

is deposited in its center, surrounded by a passive material (see Figure 7.9). When submitted to a voltage, the area of this region tends to increase up to a point where a buckling instability occurs (see Figure 7.9 (bottom)). Actuation here is non-homogeneous since one region is subjected to the voltage, while the rest of the membrane is not. We use linear elasticity and weak nonlinear equations of thin plates within the framework developed earlier to investigate the buckled morphologies.

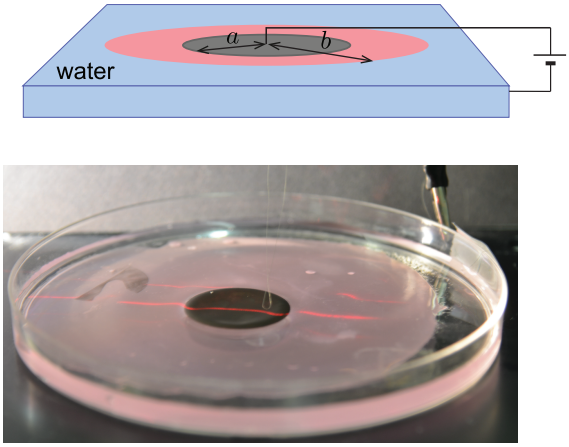

Figure 7.9. *Sketch and picture of the setup. A membrane of PVS floats freely on a bath of soapy water. A circular electrode (black circle) of radius a is connected to a high-voltage amplifier, and water is connected to the ground. When a threshold voltage has been reached, a buckling instability occurs, as can be seen from the deflected laser line on the picture. For a color version of this figure, see www.iste.co.uk/ionescu/mechatronics.zip*

7.3.3.1. *Description of the experiment*

Dielectric membranes

We use dielectric membranes made of polyvinil siloxane elastomers of Young's modulus $E = 250 \pm 15$ kPa and dielectric permittivity $\varepsilon_r = 2.5 \pm 0.6$. The polymer is spin-coated before its curing is over to obtain a circular membrane, with radius b and thickness H ranging from 100 to 300 μm. The compliant electrode consists of carbon black powder manually brushed through a circular stencil of radius a on the surface of the cured polymer. We refer to the part covered with the electrode as the *active* part, whereas the uncovered membrane is designated as the *passive* part.

This powder strongly adheres to the polymer and thus provides an electrical conductivity even when the membrane is strained at 40% (the strains we achieve experimentally are on the order of 10%).

Experimental setup

Once prepared, the membrane is gently deposited at the surface of soapy water, where it floats freely. Surfactants allow us to impose a controlled value of the surface tension $\gamma \approx 30\,\text{mN.m}^{-1}$ and enhance the electric conductivity of water. The voltage is imposed through a thin metallic wire (of radius $10\ \mu$m) in light contact with the circular electrode. The wire is connected to a high-voltage amplifier, driven by a signal generator. Water is connected to the ground and plays the role of a second compliant electrode. Voltages applied to the system typically range from 200 V to 5 kV. Out-of-plane deformations are measured with a laser sheet with a grazing incidence projected on the active part of the membrane. The deflection of the laser is recorded using a camera above the set-up and is directly proportional to the vertical displacement of the membrane. The voltage is increased by $100\,V$ every 30 s so that the experiment can be considered as quasistatic, and any viscoelastic effect of the polymer can be neglected.

7.3.3.2. *Membrane stresses below the buckling threshold*

What is the state of stress in the actuated membrane prior to buckling? We start with accounting for the effect of water surface tension. It induces a tensile strain on the order of $\gamma/EH \approx 10^{-2}$ for a 200-μm-thick membrane with free edges. We have previously shown how the electrostatic actuation could be modeled by an equivalent growth. Adapting equation [7.21] to this axisymmetric situation, the electrostatic actuation imposes a new rest length to the electrode, with an extensional strain

$$e_0 = \frac{1}{2}\frac{\varepsilon}{E}\left(\frac{V}{H}\right)^2. \qquad [7.23]$$

If we now express the strain imposed by the water surface tension, we find an equivalent voltage of $2\gamma H/\varepsilon = 700\,V$. This contribution is not negligible. However, as we are here interested in the regime below buckling, mechanics remain linear. Surface tension effects and electro-actuation are simply additive,

and therefore, we consider the pre-strained state as the reference state. Water surface tension will be taken into account when we focus on buckling and post-buckling.

If the problem is axisymmetric, the mechanical equilibrium reads:

$$\frac{\partial r\sigma_r}{\partial r} - \sigma_\theta = 0, \qquad [7.24]$$

where (r, θ) are the cylindrical coordinates, with origin the center of the membrane. σ_r and σ_θ are the radial and azimuthal stresses. In our equivalent growth approach, Hooke's relations can be written as:

$$\sigma_r = E^* \left((e_r - e_0) + \nu(e_\theta - e_0)\right) \qquad [7.25]$$

$$\sigma_\theta = E^* \left((e_\theta - e_0) + \nu(e_r - e_0)\right), \qquad [7.26]$$

with $E^* = E/(1-\nu^2)$, and $e_0 = 0$ in the passive region. Finally, noting that radial and azimuthal strains are related to the radial displacement $u(r)$ through $e_r = du/dr$ and $e_\theta = r/r$, equation [7.24] can be rewritten as:

$$r^2 u'' + ru' - u = 0, \qquad [7.27]$$

where $.'$ means the derivation with respect to r. The symmetry of the problem imposes $u(0) = 0$ and $\sigma_r(b) = 0$, while the equilibrium conditions imply the continuity of σ_r and u at the interface between the active and passive regions. With these conditions, equation [7.27] can be solved analytically to obtain the following expressions for the stress:

$$\sigma_r^A = \sigma_\theta^A = \frac{-\mathcal{P}}{2}\left(1 - \frac{a^2}{b^2}\right) < 0 \qquad [7.28]$$

$$\sigma_\theta^P = \frac{\mathcal{P}}{2}\frac{a^2}{b^2}\left(1 + \frac{b^2}{r^2}\right) > 0, \qquad [7.29]$$

with $\mathcal{P} = \frac{1}{2}\varepsilon\left(\frac{V}{H}\right)^2$. In the active region, both radial and azimuthal stresses are compressive, whereas in the passive region, only radial stresses are compressive and the azimuthal stresses are tensile. Both stresses decaying away from the active region (note also the strong discontinuity in orthoradial stress at $r = a$).

7.3.3.3. *Out-of-plane buckling*

As the voltage is increased, the active region expands in conflict with the passive region, and we have shown that radial compressive stresses build up along the whole membrane. When this stress reaches a high enough value, the membrane undergoes axisymmetric buckling. In contrast to Euler buckling, the out-of-plane deformation is strongly localized in the active region. We also note that the global mode of the instability depends on the size of the active zone (see Figures 7.10(a) and 7.10(b)). This mode, however, does not depend on the magnitude of the actuation. The superposition of the deflected laser line at different voltages in Figure 7.10 clearly shows that increasing the voltage beyond the buckling threshold only increases the amplitude of the deflection.

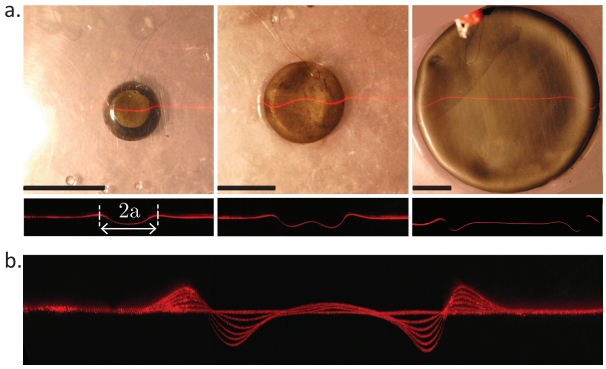

Figure 7.10. *a) Different buckling modes at $V = 5\,kV$ and $H = 210\,\mu m$ for different radii of the active zone (from left to right: $a = 0.5\,cm$, $a = 1\,cm$, and $a = 3\,cm$. The upper row is a picture of the membrane taken from above, and the lower picture highlights the profile of the membrane. The scale bar is the elastogravity length scale ($\ell_{eg} \approx 1.4\,cm$). b) Superposition of laser profiles obtained for increasing applied voltage (from 0 to $5\,kV$, $H = 210\,\mu m$, $a = 1.5\,cm$). The buckling mode does not change, only its amplitude increases. For a color version of this figure, see www.iste.co.uk/ionescu/mechatronics.zip*

The water foundation underneath the membrane introduces a new length scale that comes from the competition between gravity and bending stiffness of the plate. Balancing both effects leads to an elastrogravity length scale (Piñeirua *et al.* 2013; Pocivavsek *et al.* 2008): $\ell_{eg} = 2\pi \left(\frac{EH^3}{12(1-\nu^2)\rho g} \right)^{1/4}$, where ρ is the volumetric mass of the water, and g is the acceleration of gravity. For a typical membrane of $H = 200\,\mu$m, we obtain $\ell_{eg} \approx 1.4$ cm.

In Figure 7.10(a), we use ℓ_{eg} as a scale bar. When $a \gg \ell_{eg}$, we observe that the buckling is localized near the edges of the electrode, and the width of the corresponding annulus is comparable with this length scale (see Figure 7.10(b) (middle and right)). Conversely, when $a \leq \ell_{eg}$, the whole active region is deformed (see Figure 7.10(a), left). We assess the onset of the buckling threshold and its evolution by monitoring the profile as a function of the applied voltage (Figure 7.10). We have seen that electrostatic loading produces an actuation strain e_0 in [7.21], which we compare with the critical compressive strain for the buckling of a 1D strip lying on water $e_{1D}^c = \frac{2\pi^2}{3}(h/\ell_{eg})^2$. Results are presented in Figure 7.11. We observe a clear increase in the amplitude once a certain threshold voltage has been reached. This evolution is, however, not as sharp as in the case of a classical pitchfork bifurcation. The smoothness of the experimental transition is probably a consequence of imperfections. Among them, we can mention the slight deformation caused by the contact with the wire and the possible migration of charges outside the active region.

To describe the buckling and the post-buckling behavior, we use axisymmetric weakly nonlinear plate equations. We assume that the plate keeps a uniform thickness (strains remain low in our experiments). We use the Föppl–Von Kármán framework. We are, therefore, left with the resolution of a system of two differential equations: the in-plane equilibrium and the torque equilibrium. We do not take into account the added electrostatic bending rigidity B_V that we evidenced previously. Indeed, in this particular case, the total bending rigidity is only modified by 10% for the highest voltage accessible in our experiments. In the axisymmetric regime, the equations can be written as:

$$r^2u'' + ru' - u + \frac{1-\nu}{2}rw'^2 + r^2w'w'' = 0. \qquad [7.30]$$

$$B\Delta^2 w = N_r w'' + N_\theta \frac{w'}{r} + q \qquad [7.31]$$

with $N_r = H\sigma_r$ and $N_\theta = H\sigma_\theta$ and boundary conditions $w'(0) = w''(0) = 0$, $N_r(b) = \gamma$, $w''(0) = 0$'. Experiments and numerics are in fairly good agreement, showing the relevance of our modeling to capture this buckling instability.

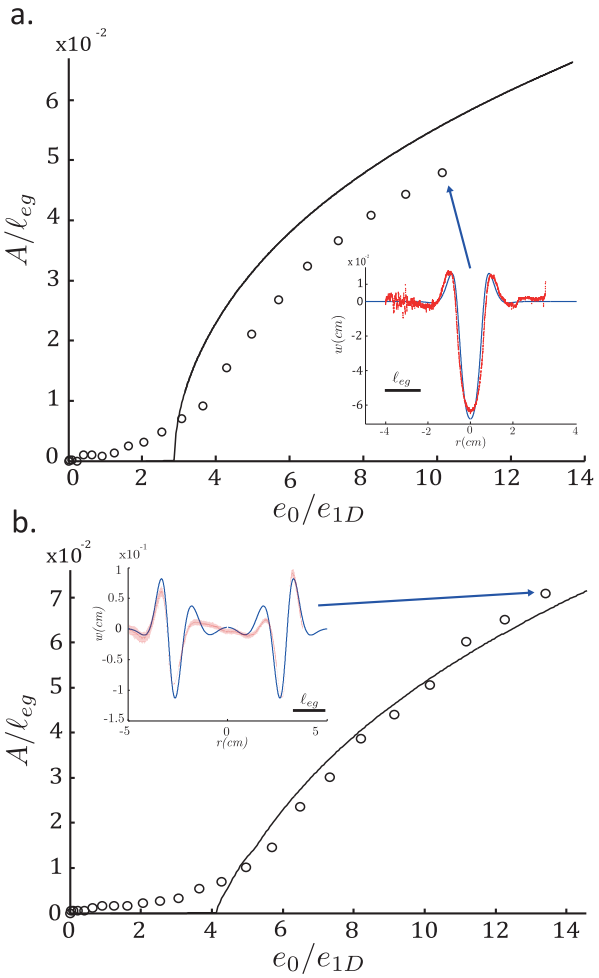

Figure 7.11. *Maximal amplitude A of the deflection normalized by ℓ_{eg} as a function of e_o/e_{1D}, where e_o is the expansion strain triggered in the active zone by electrostatic loading, and e_{1D} is the typical compressive strain leading to buckling of a 1D strip floating on water. Experimental data (circles) are compared to the numerical integration of equations [7.30] and [7.31] (continuous line). No fitting parameter. Inset: superposition of experimental (red) and numerical (profiles) at the point indicated by the arrow. a) $a = 6\,mm$. b) $a = 30\,mm$. For a color version of this figure, see www.iste.co.uk/ionescu/mechatronics.zip*

7.3.3.4. *Conclusion on dielectric elastomers*

We introduced a framework for dealing with electrostatic surface effect. In particular, we drew an analogy with biological growth. Building on this analogy, we have shown how a non-uniform voltage distribution can trigger buckling instability in a free-floating electroactive elastomer sheet. We have seen that the buckling mode depends on the size of the electrode and is set by an interplay between hydrostatics and the bending stiffness of the membrane. We also demonstrated how the framework developed in the first part, coupled with classical weakly nonlinear plate equations, allows us to capture well the behavior of the system. This tool can then be used to study the influence of the size of the electrode on the buckling threshold of the system (see Bense *et al*. 2017).

This study represents a simple demonstration of how inhomogeneous growth can trigger 3D shapes in electroactive polymers. Building on this idea, more complicated electrode geometries have been considered, which lead to different buckling modes (Hajiesmaili and Clarke 2019; Li *et al*. 2017). In parallel, numerical tools are developed to study these types of problems (see Langham *et al*. (2018)).

7.4. Conclusion

In this chapter, we discussed the effects of two different interfacial energies: one of capillary nature, and the other of electrostatic nature. On the one hand, capillary surface tension stems from the energetic cost of creating an interface (due to molecular interaction at the interface). On the other hand, an "electrostatic surface tension" can be associated with electrostatic repulsion along the surface: charges on the edge of the electrode are pushed further away by their neighbors. This analogy also helps us understand that the effects of these surface forces are contradictory: capillary surface tension tends to limit the size of the interface, while electrostatic effects favor the expansion of the electrode.

The existence of a surface energy γ brings a new length scale in elasticity $\ell_{ec} = \gamma/E$. In particular, we introduced both the elasto-capillary (with γ the liquid–vapor surface energy) and elasto-electro (with $\gamma = \frac{1}{2}\varepsilon V^2/H$) lengths that demonstrate how small the deformation produced by these surface effects are in general, even for relatively soft elastomers (a few hundreds

of kPa. Indeed, γ/E typically ranges from $10^{-7}\,m$ to $10^{-5}\,m$. It is clear that elastomer structures smaller or comparable to this length are prone to large deformations, either by capillary or by electrostatic forces. For structures made of stiff materials, we do not expect capillary nor electrostatic surface energies to generate large strains, even at the micro-scale, because γ/E is on the order of a picometer, smaller than the inter-atomic distance.

Nevertheless, we have shown that, in slender structures, the effect of small deformations may be amplified greatly. In such problems, a bending elasto-capillary length $\ell_B = \sqrt{B/\gamma}$, where B is the bending stiffness, is more relevant. When ℓ_b becomes on the order of the size of the system, surface forces are expected to generate strong bending: we have shown how a droplet may fold a thin plate and form 3D origamis through capillary forces tending to reduce the droplet surface. By contrast, electrostatic surface tension generates an expansion of the electrode. We presented a case of inhomogeneous actuation that triggers a buckling instability in a macroscopic thin plate. In both the capillary ($\ell_B \sim h^{3/2}$) and the electrostatic cases ($\ell_B \sim h^2$), the typical radius of curvature induced by surface forces l_B vanishes faster than the thickness h when a structure is scaled down: eventually, this radius of curvature becomes of the order of the structure size, leading to significant bending. We conclude that both types of surface effects become all the more important when micro- or nanostructures are considered. Such effects could be used to manipulate or efficiently actuate microstructures.

7.5. References

Andreotti, B. and Snoeijer, J. H. (in press). Statics & dynamics of soft wetting. *Annual Review of Fluid Mechanics*, 52.

Araromi, O. A., Gavrilovich, I., Shintake, J., Rosset, S., Richard, M., Gass, V., and Shea, H. R. (2015). Rollable multisegment dielectric elastomer minimum energy structures for a deployable microsatellite gripper. *ASME Transactions on Mechatronics*, 20(1), 438–446.

Bense, H., Trejo, M., Reyssat, E., Bico, J., and Roman, B. (2017). Buckling of elastomer sheets under non-uniform electro-actuation. *Soft Matter*, 13, 2876–2885, available at: http://dx.doi.org/10.1039/C7SM00131B.

Bico, J., Reyssat, E., and Roman, B. (2018). Elastocapillarity: when surface tension deforms elastic solids. *Annual Review of Fluid Mechanics*, 50(1), 629–659, available at: https://doi.org/10.1146/annurev-fluid-122316-050130.

Carpi, F., Migliore, A., Serra, G., and Rossi, D. D. (2005). Helical dielectric elastomer actuators. *Smart Materials and Structures*, 14(6), 1210, available at: http://stacks.iop.org/0964-1726/14/i=6/a=014.

Carpi, F. and Rossi, D. D. (2007). Bioinspired actuation of the eyeballs of an android robotic face: Concept and preliminary investigations. *Bioinspiration & Biomimetics*, 2(2), S50–S63, available at: http://stacks.iop.org/1748-3190/2/i=2/a=S06?key=crossref.b7fe86d7b650c6fd1d3b23dd6fc97ed8.

Carpi, F., Frediani, G., Turco, S., and De Rossi, D. (2011). Bioinspired tunable lens with muscle-like electroactive elastomers. *Advanced Functional Materials*, 21(21), 4152–4158, available at: http://doi.wiley.com/10.1002/adfm.201101253.

Cho, J.-H., Datta, D., Park, S.-Y., Shenoy, V. B., and Gracias, D. H. (2010). Plastic deformation drives wrinkling, saddling, and wedging of annular bilayer nanostructures. *Nano Letters*, 10(12), 5098–5102, available at: http://pubs.acs.org/doi/abs/10.1021/nl1035447.

de Gennes, P., Brochard-Wyart, F., and Quéré, D. (2002). *Gouttes, bulles, perles et ondes*. Collection Échelles, Belin, available at: https://books.google.nl/books?id=Y6KOAAAACAAJ.

Dervaux, J. and Ben Amar, M. (2008). Morphogenesis of growing soft tissues. *Physical Review Letters*, 101, 068101, available at: https://link.aps.org/doi/10.1103/PhysRevLett.101.068101.

Foo, C., Koh, S. J. A., Keplinger, C., Kaltseis, R., Bauer, S., and Suo, Z. (2012). Performance of dissipative dielectric elastomer generators. *Journal of Applied Physics*, 111(9), 094107.

Hajiesmaili, E. and Clarke, D. R. (2019). Reconfigurable shape-morphing dielectric elastomers using spatially varying electric fields. *Nature Communications*, 10(1), 183, available at: https://doi.org/10.1038/s41467-018-08094-w.

Huang, J., Li, T., Chiang Foo, C., Zhu, J., Clarke, D. R., and Suo, Z. (2012). Giant, voltage-actuated deformation of a dielectric elastomer under dead load. *Applied Physics Letters*, 100(4), 041911, available at: https://doi.org/10.1063/1.3680591.

Hui, C. Y., Jagota, A., Lin, Y. Y., and Kramer, E. J. (2002). Constraints on microcontact printing imposed by stamp deformation. *Langmuir*, 18(4), 1394–1407, available at: http://pubs.acs.org/doi/abs/10.1021/la0113567.

Kaltseis, R., Keplinger, C., Baumgartner, R., Kaltenbrunner, M., Li, T., Mächler, P., Schwädiauer, R., Suo, Z., and Bauer, S. (2011). Method for measuring energy generation and efficiency of dielectric elastomer generators. *Applied Physics Letters*, 99(16), 162904, available at: https://doi.org/10.1063/1.3653239.

Keplinger, C., Kaltenbrunner, M., Arnold, N., and Bauer, S. (2010). Röntgen's electrode-free elastomer actuators without electromechanical pull-in instability. *Proceedings of the National Academy of Sciences*, 107(10), 4505–4510, available at: https://www.pnas.org/content/107/10/4505.

Kim, J., Hanna, J. A., Byun, M., Santangelo, C. D., and Hayward, R. C. (2012). Designing responsive buckled surfaces by halftone gel lithography. *Science*, 335(6073), 1201–1205, available at: https://science.sciencemag.org/content/335/6073/1201.

Klein, Y., Efrati, E., and Sharon, E. (2007). Shaping of elastic sheets by prescription of non-euclidean metrics. *Science*, 315(5815), 1116–1120, available at: https://science.sciencemag.org/content/315/5815/1116.

Langham, J., Bense, H., and Barkley, D. (2018). Modeling shape selection of buckled dielectric elastomers. *Journal of Applied Physics*, 123(6), 065102, available at: https://doi.org/10.1063/1.5012848.

Lester, G. (1961). Contact angles of liquids at deformable solid surfaces. *Journal of Colloid Science*, 16(4), 315–326, available at: http://www.sciencedirect.com/science/article/pii/0095852261900320.

Li, K., Wu, W., Jiang, Z., and Cai, S. (2017). Voltage-induced wrinkling in a constrained annular dielectric elastomer film. *Journal of Applied Mechanics*, 85(1), 011007–011017, available at: http://dx.doi.org/10.1115/1.4038427.

Lippmann, G. (1875). Relations entre les phénomènes électriques et capillaires. PhD thesis, Faculté des sciences de Paris, Paris.

Love, A. E. H. (2011). *A Treatise on the Mathematical Theory of Elasticity*. Dover editions, USA.

Maffli, L., Rosset, S., Ghilardi, M., Carpi, F., and Shea, H. (2015). Ultrafast all-polymer electrically tunable silicone lenses. *Advanced Functional Materials*, 25(11), 1656–1665, available at: https://onlinelibrary.wiley.com/doi/abs/10.1002/adfm.201403942.

McKay, T. G., O'Brien, B. M., Calius, E. P., and Anderson, I. A. (2011). Soft generators using dielectric elastomers. *Applied Physics Letters*, 98(14), 142903, available at: https://doi.org/10.1063/1.3572338.

Mora, S., Maurini, C., Phou, T., Fromental, J.-M., Audoly, B., and Pomeau, Y. (2013). Solid drops: Large capillary deformations of immersed elastic rods. *Physical Review Letters*, 111(11), 114301, available at: http://link.aps.org/doi/10.1103/PhysRevLett.111.114301.

Namatsu, H., Kurihara, K., Nagase, M., Iwadate, K., and Murase, K. (1995). Dimensional limitations of silicon nanolines resulting from pattern distortion due to surface tension of rinse water. *Applied Physics Letters*, 66(20), 2655–2657, available at: https://doi.org/10.1063/1.113115.

Patra, N., Wang, B., and Král, P. (2009). Nanodroplet activated and guided folding of graphene nanostructures. *Nano Letters*, 9(11), 3766–3771, available at: https://doi.org/10.1021/nl9019616.

Pelrine, R., Kornbluh, R., and Joseph, J. (1998). Electrosctriction of polymer dielectrics with compliant electrodes as a means of actuation. *Sensors and Actuators A*, 64, 77–85.

Piñeirua, M., Tanaka, N., Roman, B., and Bico, J. (2013). Capillary buckling of a floating annulus. *Soft Matter*, 9, 10985–10992, available at: http://dx.doi.org/10.1039/C3SM51825F.

Pocivavsek, L., Dellsy, R., Kern, A., Johnson, S., Lin, B., Lee, K. Y. C., and Cerda, E. (2008). Stress and fold localization in thin elastic membranes. *Science*, 320(5878), 912–916, available at: https://science.sciencemag.org/content/320/5878/912.

Py, C., Reverdy, P., Doppler, L., Bico, J., Roman, B., and Baroud, C. N. (2007). Capillary origami: Spontaneous wrapping of a droplet with an elastic sheet. *Physical Review Letters*, 98, 156103, available at: https://link.aps.org/doi/10.1103/PhysRevLett.98.156103.

Shintake, J., Rosset, S., Schubert, B., Floreano, D., and Shea, H. (2016). Versatile soft grippers with intrinsic electroadhesion based on multifunctional polymer actuators. *Advanced Materials*, 28(2), 231–238.

Son, S.-i., Pugal, D., Hwang, T., Choi, H. R., Koo, J. C., Lee, Y., Kim, K., and Nam, J.-D. (2012). Electromechanically driven variable-focus lens based on transparent dielectric elastomer. *Applied Optics*, 51(15), 2987–2996, available at: http://ao.osa.org/abstract.cfm?URI=ao-51-15-2987.

Style, R. W., Boltyanskiy, R., Che, Y., Wettlaufer, J. S., Wilen, L. A., and Dufresne, E. R. (2013). Universal deformation of soft substrates near a contact line and the direct measurement of solid surface stresses. *Physical Review Letters*, 110, 066103, available at: https://link.aps.org/doi/10.1103/PhysRevLett.110.066103.

Tas, N., Vogelzang, B., Elwenspoek, M., and Legtenberg, R. (1997). *Adhesion and Friction in MEMS*. Springer Netherlands, Dordrecht, pp. 621–628.

Wu, Z. L., Moshe, M., Greener, J., Therien-Aubin, H., Nie, Z., Sharon, E., and Kumacheva, E. (2013). Three-dimensional shape transformations of hydrogel sheets induced by small-scale modulation of internal stresses. *Nature Communications*, 4, 1586, available at: https://doi.org/10.1038/ncomms2549.